JMME. Vol. 11 September 2018 *ISSN: 2006-1919*
pp. 77-86

CRYSTALLOGRAPHIC TEXTURE-DEPENDENT DISSOLUTION OF THERMOMECHANICALLY PROCESSED BIODEGRADABLE PURE IRON

Camillus S. Obayi[1, 2], Paul S. Nnamchi[1], Ranna Tolouel[2], Boniface A. Okorie[1], Diego Mantovani[2]

[1] Department of Metallurgical & Materials Engineering, University of Nigeria, Nsukka, Nigeria
[2]Laboratory for Biomaterials and Bioengineering, Department of Materials Engineering &University Hospital Research Centre, Laval University, Quebec City, G1K 7P4, Canada.

ABSTRACT

Low *in vivo* dissolution rate is a major setback in the use of pure iron (Fe) as a biodegradable metallic implant material. Many methods employed to overcome this major limitation modify microstructure, which in turn moderate dissolution kinetics. Crystallographic texture is one of such microstructural parameters. This work demonstrates a relationship between the texture strength of crystallographic planes and the *in vitro* dissolution rate of pure Fe in simulated body fluid (Hanks' solution). Pure Fe samples were subjected to thermomechanical processing-cold rolling and recrystallization annealing. The developed crystallographic textures were characterized with X-ray diffractometer (XRD). The corrosion rates were determined in Hank's solution using Potentiodynamic polarization test. The result indicated that the deformation textures which were predominantly {200}, reverted to different intensities of {110}, {200} and {211} after recrystallization annealing. (110), (200) and (211) textures had significant effects on the corrosion current density. Corrosion current increased as the texture strengths of (110) and (211) increased, but decreased as the texture strength of (200) increased. For enhanced dissolution rate, a processing technique that would lead to increase and decrease in texture strengths of (110) and (200) respectively in pure iron should be sought.

Keywords: crystallographic texture, texture strength, biodegradable metal, dissolution rate, pure iron, Hank's solution

1.0 INTRODUCTION

Pure iron (>99.8% Fe) has attracted an extensive research effort since its first investigation as a biodegradable metal (BM) for cardiovascular stent application in 2001 [1]. However, a low *in vivo* dissolution rate was observed as a major setback for its potential use as a biodegradable stent material. This pioneer work recommended alloying or surface and structural modification as a valuable approach to overcoming this major limitation and achieving a faster degradation rate [1]. Thus, post 2001 research efforts by the Fe-based BM community have targeted uniform accelerated degradation and enhanced mechanical properties, in addition to improved biocompatibility of pure iron using various methods.

Some of the methods exploited so far include alloying [2, 3, 4, 5, 6], electroforming [7], equal channel angle pressure (ECAP) technique [8], composite preparation [9] and surface modification [10, 11, 12, 13], including the recently reported patterning of pure Fe surface with Platinum disc arrays [14]. All these techniques affect microstructure developed in pure Fe both in the bulk and on the surface. And the degradation behaviour is usually interpreted based on the alloy chemistry, without taking into consideration the microstructural parameters that drive/support the chemical

kinetics. The microstructural parameters affected include the crystallographic texture (preferred orientation of grains), grain size, grain shape and their distribution in the microstructure, which singly or collectively moderate the degradation kinetics of pure Fe. Research has shown that crystallographic texture affects the dissolution, corrosion or oxidation of metals [15, 16, 17, 18, 19, 20] as evidenced by the results of some authors who have investigated the effect of crystallographic textures of (111), (101) and (100) planes on corrosion behaviour of single and nano-crystalline Fe crystals in various non-biological media [21, 22, 23, 24, 25, 26]. The general conclusions from these investigations on dissolution behaviour of Fe-based metals in various non-physiological media are that (111) plane has the highest atomic packing density, the highest dissolution rate and the most resistant against pitting corrosion while (100) plane has the lowest atomic packing density, the most corrosion resistant and less resistant against pitting corrosion. Among the authors who have studied the effect of texture on corrosion of pure Fe in Hank's solution are Moravej, et al [27] and Obayi, et al [28], who investigated the effects of current density and cross rolling on the microstructure and texture development in electroformed Fe and cross rolled pure Fe, respectively. Moravej, et al found out that current density influenced the texture development in pure Fe and electrodeposited pure Fe with strong (111) texture showed a uniform corrosion higher than that of Armco® iron. On the other hand, the result of Obayi, et al, showed that there were only marginal differences in the degradation rates between pure Fe unidirectional rolled and cross-rolled to 75% reduction after annealing. However, none of these studies indicated the correlation between dissolution behaviour and texture strength.

In this context, there is the need to investigate the effect of other manufacturing methods on texture development and dissolution of pure Fe, particularly thermomechanical processing (plastic deformation and annealing) which is a stent manufacturing step. From this perspective, this investigation is aimed at demonstrating the relationship between the preferred crystallographic textures (planes) developed during the thermomechanical processing and *in vitro* corrosion behaviour of pure Fe in Hank's solution. This investigation will add to the emerging knowledge on the effect of microstructure on degradation behaviour of BM and aid in further understanding of the mechanism of pure Fe degradation from microstructural point of view.

2.0 EXPERIMENTAL DETAILS

The pure iron used in this work was supplied by Good fellow Limited, Cambridge, United Kingdom. The pure iron was an Armco® soft ingot iron (>99.8% purity) in the form of 2 mm thick as-rolled sheets. Its chemical composition (wt. %) was determined in a previous work [29].

Samples were cut from the 2 mm-thick pure iron sheets and undirectionally cold rolled to 50% (UD50%CR), 75% (UD75%CR) and 85% (UD85%CR) thickness reduction to achieve 1 mm, 0.5 mm and 0.3 mm thicknesses, respectively. Rolling was done using a Stanat two-high rolling mill (Stanat, Rolling Mill; model TA-315), having 130 mm work rolls. The cold-rolled samples were recrystallization annealed in a tube furnace in the temperature range of 550°C - 900°C, under a high purity argon atmosphere using a heating rate of 6.5°C per minute. During recrystallization annealing, the specimens were soaked for two hours and air cooled.

The average texture and preferred crystallographic orientation of the samples on rolling surface or normal direction (ND) were analyzed using Siemens D5000 X-ray diffractometer (Siemens AG, Germany).

The diffractometer was operated using Cu-Kα radiation (λ = 0.15406 nm) at an accelerating voltage of 40 kV and a current of 30 mA. The scan rate was 0.05 °.s^{-1} in the range of 20-120° at a step size of 0.02°. The texture strength or fraction of grains in a specific orientation was determined by calculating the ratios of the peak intensities of the experimental material to the peak intensities of the reference material. Then the texture strength, P_{hkl} of the three major orientations of grains on the rolling surface was calculated using the following equations (1-3) [30]:

$$P_{(110)} = \frac{\frac{i_{110}}{I_{110}}}{\frac{i_{110}}{I_{110}} + \frac{i_{200}}{I_{200}} + \frac{i_{211}}{I_{211}} + \frac{i_{220}}{I_{220}}} \quad \ldots\ldots\ldots 1$$

$$P_{(200)} = \frac{\frac{i_{200}}{I_{200}}}{\frac{i_{110}}{I_{110}} + \frac{i_{200}}{I_{200}} + \frac{i_{211}}{I_{211}} + \frac{i_{220}}{I_{220}}} \quad \ldots\ldots\ldots 2$$

$$P_{(211)} = \frac{\frac{i_{211}}{I_{211}}}{\frac{i_{110}}{I_{110}} + \frac{i_{200}}{I_{200}} + \frac{i_{211}}{I_{211}} + \frac{i_{220}}{I_{220}}} \quad \ldots\ldots\ldots 3$$

where i_{110}, i_{200}, i_{211} are the intensities of the (hkl) Bragg peak from the experimental material and I_{110}, I_{200}, I_{211} are the intensities of the (hkl) reflection from the reference material listed in the Joint Committee on Powder Diffraction Standards (JCPDS) card of body-centred cubic (bcc) iron (JCPDS card 6-696).

Potentiodynamic polarization test was used to assess the *in vitro* biodegradation behaviour of samples in a modified Hanks' solution. The Potentiodynamic polarization test was performed using a conventional three-electrode cell (VersaSTAT3 potentiostat/galvanostat system, Princeton Applied Research, USA). The specimen, a graphite electrode and a saturated calomel electrode (SCE) were set as the working electrode, auxiliary/counter electrode and reference electrode, respectively. The test coupons were cut, wet polished using SiC papers from 120 down to 4000 grit and subsequently cleaned with ethanol and dried in warm air. The area of the polished disc-shaped working electrode exposed to the test solution was 0.16 cm^2. The test solution was modified Hanks' solution, which the ionic composition and concentration were presented in Ref [31]. All corrosion tests were performed in 650 ml of stirred Hank's solution having a pH of 7.4 and temperature thermostatically maintained at 37±1°C. The open circuit potential (OCP) measurement was maintained up to 3600 s. The Potentiodynamic polarization test was carried out in the potential range -1000 mV (vs. SCE) to -250 mV (vs. SCE) at a scanning rate of 0.166 mV.s^{-1}. The corrosion rate (CR) was calculated using equation (4) based on ASTM G59 [32].

$$CR = 3.27x10^{-3}\frac{i_{corr.}EW}{\rho} \quad \ldots\ldots\ldots 4$$

where *CR* is the corrosion rate in millimetre per year (mm/yr), i_{corr} is the corrosion current density (μA/cm^2) deduced from Tafel curves, *EW* is the equivalent weight (27.92 g/eq for Fe) and ρ is the density (g/cm^3).

Statistical analysis was performed to determine the significant effects of the crystallographic texture on the dissolution rates of pure Fe samples using one-way analysis of variance (ANOVA) and significance level were considered at $p \leq 0.05$ and P-values less than 0.05 were considered to be statistically significant.

3.0 RESULTS AND DISCUSSION

3.1 Texture evolution

The texture development after cold rolling and the accompanying changes after the process of recrystallization annealing are shown in Figures 1-4. Figure 1 shows the X-ray diffraction (XRD) patterns of the surface layers of the as-received and as-rolled pure iron samples (UD50%CR, UD75%CR, UD85%CR). Figure 2 displays

the annealing diffractograms of some of the pure iron samples. The positions of the three predominant diffraction peaks {(110), (200) and (211)}in the XRD diffractograms remain constant indicating that the lattice parameters were unchanged and no new phases were formed in the samples. The calculated texture index corresponding to three predominant peaks in the diffractograms of Figures 1-2 are listed in Tables 1-2. The plots of the texture index of the pure iron samples in as-rolled and in annealed conditions are illustrated in Figure 3 and Figure 4, respectively. The texture index is used to quantify the texture strength or is a measure of the extent or degree of preferred orientation of the grains.

From the calculated texture strength, all the as-cold rolled pure Fe samples (UD50%CR, UD75%CR, UD85%CR) have a predominant cold rolling texture or preferred orientation of (200) as shown in Figure 3. This rolling texture evolution is in agreement with rolling texture evolution in body-centred cubic metals which predominantly consists of (100) planes oriented parallel to the plane of the sheet [33]. The as-rolled texture index of the (200) decreased with increase in the degree of cold rolling. It also increased with increase in annealing temperatures. The first rapid development of {200} textures in rolled samples with increasing deformation had been observed in cold rolling of iron and low carbon steel [34].

The annealed samples were code-named according to the degree of cold rolling and heat treatment temperature as viz: UD50%CR-550, UD50%CR-900, UD75%CR-550, UD75%CR-900, UD85%CR-550 and UD85%CR-900, respectively. On heat treatment, the as-rolled texture reverted to different intensities of {110}, {200} and {211}, depending on the amount of cold work and annealing temperatures (Figure 4). The preferred recrystallization textures of the annealed pure iron samples at 550ºC (UD75%CR-550°C and UD85%CR-550°C) were that of (110) and were slightly above that of the as-received. However, at 900°C, the preferred orientation of (UD75%CR-900°C) sample reverted to (200) texture. The predominance of {110} texture at 550ºC on recrystallization could be explained in terms of variation of stored energy of deformation which increases from {100} to {110} [35, 36]. {110} texture stores more energy leading to its retention at 550ºC and its conversion to lower energy storing texture of {200} at higher temperature. This result is in agreement with the work of Schreiber and co-workers [15] where annealing of polycrystalline iron led to a change in the distribution of grain orientations in favour of (101) and (111) oriented grains, and less of (100) oriented grains.

The preferred orientation of UD50%CR (200) persisted, its texture index decreased at 550ºC and increased slightly at 900ºC.

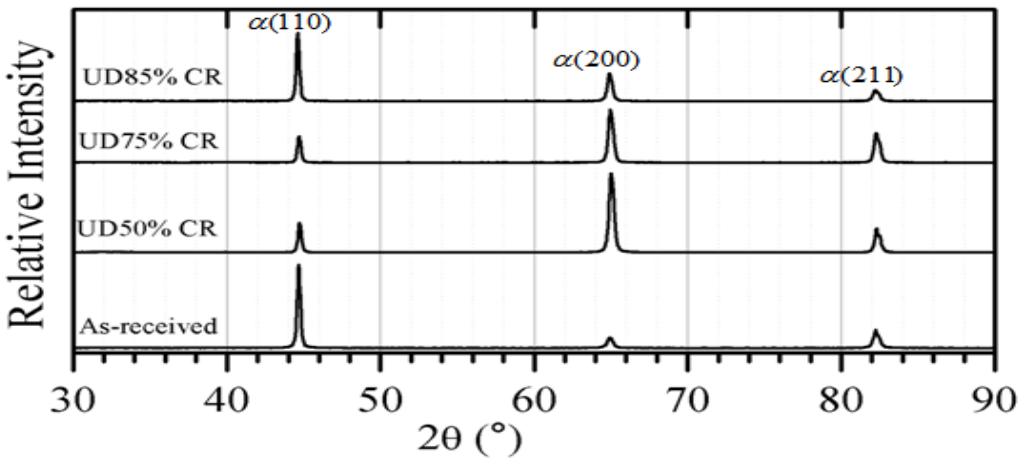

Figure 1: *As-rolled diffractograms of the pure Fe samples.*

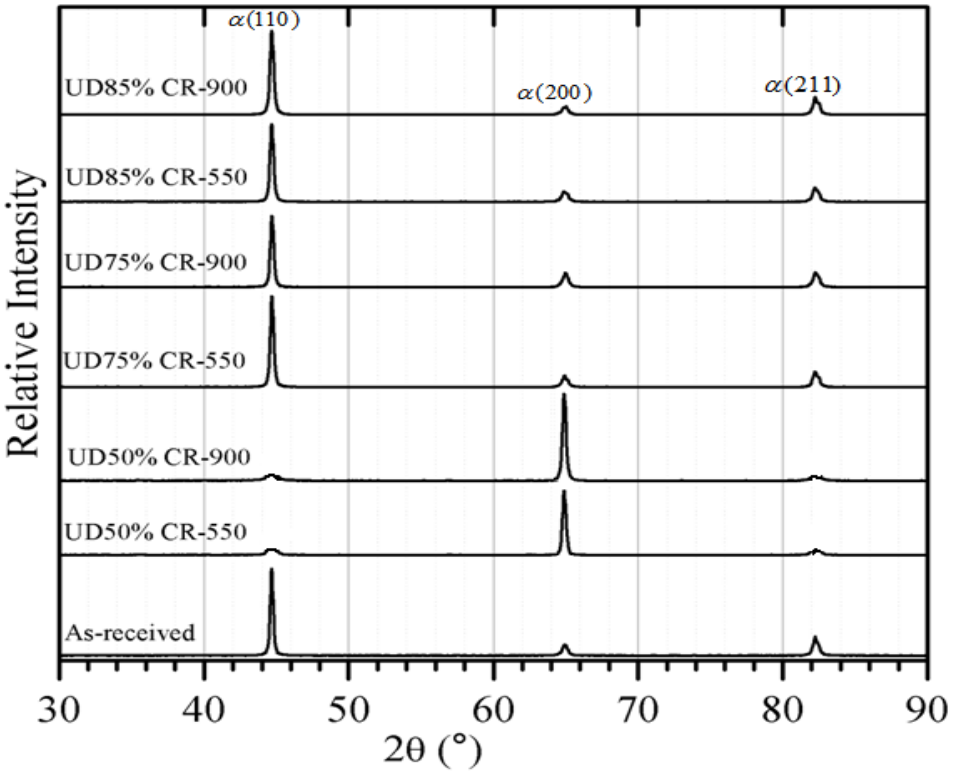

Figure 2: Annealing diffractograms of the pure Fe samples.

Table 1: Calculated texture index and preferential orientations of the as-received and as-rolled pure Fe samples.

	Texture Index			Preferential orientation
Material code	**(110)**	**(200)**	**(211)**	
As-received	1.1033	0.9239	0.8454	110
UD50%CR	0.3369	6.1781	0.9798	200
UD75%CR	0.3662	5.0260	1.4691	200
UD85%CR	0.9503	2.6290	0.5379	200

Table 2: Calculated texture index and preferential orientations of the as-received and some of the annealed pure Fe samples.

	Texture Index			Preferential orientation
Material code	**(110)**	**(200)**	**(211)**	
As-received	1.1033	0.9239	0.8454	110
UD50%CR-550	0.0202	9.2026	0.0321	200
UD50%CR-900	0.0093	10.1633	0.0222	200
UD75%CR-550	1.1434	0.9941	0.6896	110
UD75%CR-900	1.0454	1.4621	0.7728	200
UD85%CR-550	1.1341	0.7684	0.8593	110
UD85%CR-900	1.1241	1.0405	0.7234	110

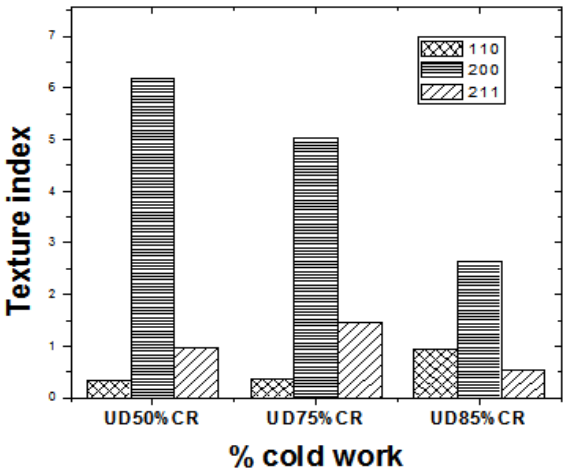

Figure 3: *As-rolled texture index of the pure Fe samples.*

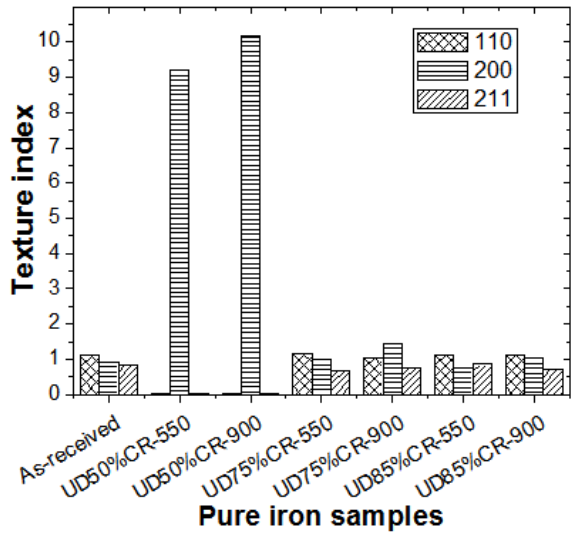

Figure 4: *Texture index of the as-received and some of the heat-treated pure iron samples.*

3.2 Corrosion behaviour.

Figure 5 shows Potentiodynamic polarization curves of the as-received and some of the annealed pure Fe samples, obtained during Potentiodynamic polarization corrosion test. The anodic and cathodic polarization curves of the pure Fe samples are similar which suggests that similar corrosion mechanism occurred in all the samples. Figure 6 illustrates the relationship between texture strength and corrosion current density for annealed pure Fe samples. Table 3 is summary of the corrosion data obtained from Potentiodynamic polarization and the effect of recrystallization texture on the corrosion properties of the as-received and some of the annealed pure iron samples. The results of the ANOVA also indicate that crystallographic texture {(110) (P = 0.00056), (200) (P = 0.00033), (211) (P = 0.00094)} have significant effects on the corrosion current density (I_{corr}) as P values are less than 0.05. The corrosion current density (I_{corr}) of the pure Fe samples increased with increase in the texture strength of (110) and (211), but decreased with increase in the texture strength of (200).

In BCC iron, (110) crystal faces are more closely packed and have higher atomic density than (100) crystal faces. Closely packed faces of pure Fe had been found to be more susceptible to dissolution in acetate buffer solution (pH 6.0) than loosely-packed crystal faces (100) which were the most corrosion resistant and had strongest oxide formation tendencies [15]. This is because the distance to the next layer in a closely packed plane is larger and the surface atoms are less strongly bound, thereby making (110) grains more susceptible to active dissolution than the (100) planes. The reduced corrosion rate of pure Fe samples with (100) crystal faces could also be attributed to their relatively low surface energy [37]. Thus, an increase in texture index of (110) plane is an increase in atomic density and surface energy while a decrease in texture strength of (200) implied a decrease in oxide formation tendencies [15, 38], which made the pure iron samples more susceptible to dissolution in the corrosive media [39].

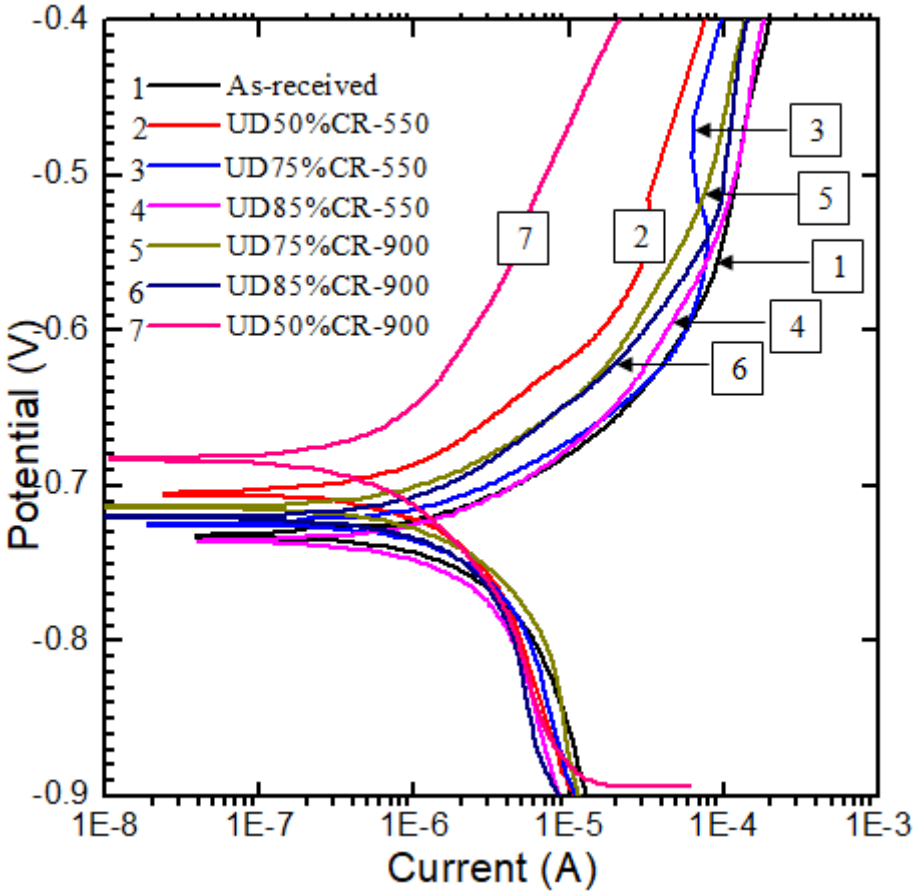

Figure 5: *Potentiodynamic polarization curves of the as-received and some annealed pure iron samples*

Table 3: Summary of the effect of crystallographic texture on the corrosion properties of the as- received and some of the annealed pure iron samples.

Material code	**Texture index**				**Potentiodynamic polarization test**		
	(110)	(200)	(211)	Preferential orientation	Corrosion potential (mV)	Current density I_{corr} (µA cm^{-2})	Corrosion rate (mm $year^{-1}$)
As-received	1.1033	0.9239	0.8454	110	-732 ± 3	20.89 ± 0.6	0.242 ± 0.010
UD50%CR-550-A	0.0202	9.2026	0.0321	200	-704±5	14.41±0.7	0.167±0.011
UD50%CR-900-A	0.0093	10.1633	0.0222	200	-682±3	13.33±1.0	0.155±0.019
UD75%CR-550-A	1.1434	0.9941	0.6896	110	-724 ± 4	20.9 ± 1.8	0.243 ± 0.029
UD75%CR-900-A	1.0454	1.4621	0.7728	200	-720 ± 6	19.50 ± 1.5	0.226 ± 0.024
UD85%CR-550-A	1.1341	0.7684	0.8593	110	-736±3	21.56±0.5	0.250±0.030
UD85%CR-900-A	1.1241	1.0405	0.7234	110	-726±7	20.05±0.9	0.233±0.015

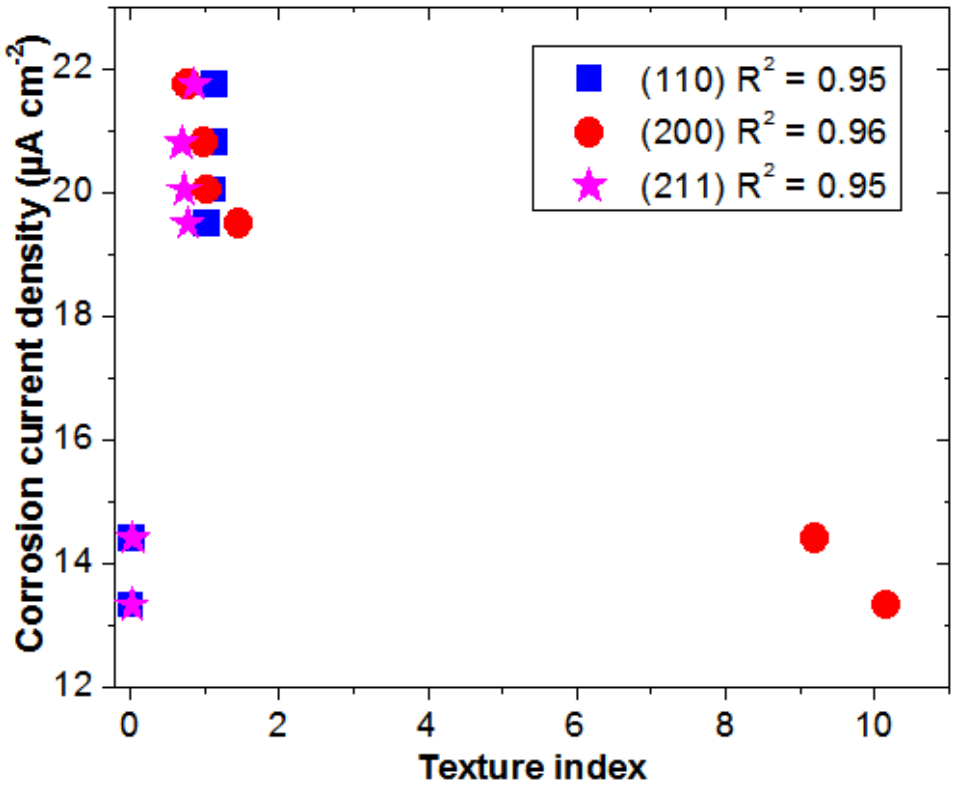

Figure 6: *The relationship between texture strength and corrosion current density for annealed pure Fe samples (R^2>0.9).*

4.0 CONCLUSION

The effect of crystallographic texture on the dissolution behaviour of pure Fe in simulated body fluid has been investigated. The as-rolled or deformation texture in pure iron samples was predominantly {200}, but this texture strength decreased with increase in the amount of cold work. During recrystallization annealing, the as-rolled texture reverted to different intensities of {110}, {200} and {211}, depending on the amount of cold work and annealing temperatures. The predominant annealing textures in the samples were that of {110} after heat treatment at 550ºC, which reverted to {200} after heat treatment at 900ºC. (110), (200) and (211) textures had significant effects on the corrosion current density. Corrosion current density increased as the texture indexes of (110) and (211) increased, but decreased as the texture index of (200) increased. Structural modification that would lead to increase and decrease in texture strengths of (110) and (200) in pure iron, respectively, should be sought for enhanced dissolution rate of pure iron.

ACKNOWLEDGEMENTS

This work was partially supported by NSERC-Canada, CIHR-Canada, CFI-Canada, FRQ-NT-Quebec, MRI-Quebec, Canadian Commonwealth Scholarship Program and University of Nigeria, Nsukka.

REFERENCES

1. Peuster M, Wohlsein P, Brügmann M, Ehlerding M, Seidler K, Fink C, et al. A novel approach to temporary stenting: degradable cardiovascular stents produced from corrodible metal—results 6–18 months after implantation into New Zealand white rabbits. Heart 2001, 86, 563–569.

2. Hermawan, H.; Alamdari, H.; D. Mantovani; Dominique Dube; Iron-manganese: new class of metallic degradable biomaterials prepared by

powder metallurgy. Powder Metallurgy. 2008, **51**(1): 38-45.

3. Schinhammer, M.; Anja C. Hanzi; Jorg F. Loffler; Peter J. Uggowitzer. Design strategy for biodegradable Fe-based alloys for medical applications. Acta Biomaterialia. 2010, **6**(5): 1705-1713.
4. Liu, B.; Y.F. Zheng. Effects of alloying elements (Mn, Co, Al, W, Sn, B, C and S) on biodegradability and in vitro biocompatibility of pure iron. Acta Biomaterialia. 2011, **7**(3): 1407-1420.

5. Liu, B.; Y.F. Zheng; L. Ruan. In vitro investigation of Fe30Mn6Si shape memory alloy as potential biodegradable metallic material. Materials Letters. 2010, 65(3): 540-543.

6. Michael Schinhammer; Patrick Steiger; Frank Moszner; F. L¨offler; Peter J. Uggowitzer. Degradation performance of biodegradable Fe–Mn–C (-Pd) alloys, Materials Science & Engineering C. 2012, doi: 10.1016/j.msec.2012.10.013.

7. M. Moravej; F.Prima; M. Fiset; D. Mantovani. Electroformed iron as new biomaterial for degradable stents: Development process and structure-properties relationship. Acta Biomaterialia. 2010, **6**(5): 1726-1735.

8. F.L. Nie; Y.F. Zheng; S.C. Wei; C. Hu; G. Yang. In vitro Corrosion, Cytotoxicity and Hemocmpatibility of Bulk Nanocrystalline Pure Iron. Biomedical Materials. 2010, 5, 065015.

9. Cheng, J., Zheng, Y. *In vitro* study on newly designed biodegradable Fe-X composites (X=W, CNT) prepared by spark plasma sintering. Journal of Biomedical Materials Research Part B: Applied Biomaterials 101B, 2013, 485-497.

10. Zhu, S.; Huang N.; Xu L.; Zhang Y.; Liu H,; Lei Y.; Sun H.; Yao Y. Biocompatibility of Fe-O films synthesized by plasma immersion ion implantation and deposition. Surface and Coatings Technology. 2009, **203**(10-11): 1523-1529.

11. Shengfa Zhu; Nan Huang; Hui Shu; Yanping Wu; Li Xu. Corrosion resistance and blood compatibility of lanthanum ion implanted pure iron by MEVVA. Applied Surface Science. 2009, **256**(1): 99-104.

12. Chen Chang-Zi, Shi Xing-Hua, Zhang Peng-Cheng, Bin Bai, Leng Yong-Xiang, Nan Huang, The microstructure and properties of commercial pure iron modified by plasma nitriding. Solid State Ionics, 2008, 179, 971–974.
13. Chen, H., Zhang, E., Yang, K. Microstructure, corrosion properties and biocompatibility of calcium zinc phosphate coating on pure ion for biomedical application. Materials Science and Engineering C, 2014, 34, 201-206.

15. Tao Huang, Yufeng Zheng, Uniform and accelerated degradation of pure iron patterned by Pt disc arrays, Scientific Reports, 2016 | 6:23627 | DOI: 10.1038/srep23627

15. A. Schreiber; J.W. Schultze; M.M. Lohrengel; F. K´arm´an; E. K´alm´an. Grain dependent electrochemical investigations on pure iron in acetate buffer pH 6.0, ElectrochimicaActa. 2006, 51, 2625–2630.

16. Ming, Liu; Dong Qiu; Ming-Chun Zhao; Guangling Song; Andrej Atrens. The effect of crystallographic orientation on the active corrosion of pure magnesium. Scripta Materialia. 2008, 58, 421-424.

17. S. J. Splinter, R. Rofagha, N. S. McIntyre, U. Erb. XPS Characterization of the Corrosion Films Formed on Nanocrystalline Ni–P Alloys in Sulphuric Acid. Surface & Interface Analysis, 1996, 24, 181-186.

18. Yong Choi, Hirofumi Inoue. Crystallographic texture development and its effect on corrosion behaviour of pilgered Zirconium alloy tube. Materials Transactions, 2010, 51(4), 652-658.

19 J.W. Schultze, B. Davepon, F. Karman, C. Rosenkranz, A. Schreiber, O. Voigt. Corrosion & Passivation in Nanoscopic & Microscopic Dimensions: The Influence of Grains & Grain Boundaries. Corros. Eng. Sci. & Technol. 2004, 39 (1), 45-52.

20 Majid Hoseini, Arash Shahryari, Sasha Omanovic, Jerzy A. Szpunar, Comparative effect of grain size and texture on the corrosion behaviour of commercially pure titanium processed by equal channel angular pressing, Corrosion Science, 2009, 51 (12), 3064–3067.

21. Wang, S G; Shen, C B; Long, K; Yang H Y; Wang F H; Zhang, Z D. Preparation and Electrochemical Corrosion Behavior of Bulk Nanocrystalline Ingot Iron in HCl Acid

Solution. The Journal of Physical Chemistry B. 2005, 109(7): 2499-2503.

22. Afshari, V., C. Dehghanian. Effects of grain size on the electrochemical corrosion behaviour of electrodeposited nanocrystalline Fe coatings in alkaline solution. Corrosion Science. 2009. 51(8): 1844-1849.

23. Afshari, V.; C. Dehghanian. Electrochemical polarization and passivation of Nanostructured iron in acid solution, Anti-Corrosion Methods and Materials, 2010. 57 (3), 142-147.

24. W. Zeiger; M. Schneider; H. Worch.Passivity and Pitting Corrosion of a Nanocrystalline FeAl8-Alloy,Materials Science Forum. 1998, Vol. 269 – 272, 833-836.

25. Wang, X.Y.; D.Y. Li. Mechanical and electrochemical behavior of nanocrystalline surface of 304 stainless steel. Electrochimica Acta. 2002, 47(24): 3939-3947.

26. X.Y. Wang; D.Y. Li. Mechanical, electrochemical and tribological properties of nano-crystalline surface of 304 stainless steel, Wear. 2003. 255, 836–845.

27. Maryam Moravej, Sofiene Amira, Frédéric Prima, Ahmed Rahem, Michel Fiset, Diego Mantovania. Effect of electrodeposition current density on the microstructure and the degradation of electroformed iron for degradable stents. Materials Science and Engineering B, 2011, 176(20), 1812-1822.

28. Camillus Sunday Obayi, Ranna Tolouei, Carlo Paternoster, Stephane Turgeon, Boniface Adeleh Okorie, Daniel Oray Obikwelu, Glenn Cassar, Joseph Buhagiar, Diego Mantovani. *Influence of cross-rolling on the micro-texture and biodegradation of pure iron as biodegradable material for medical implants*, Acta Biomaterialia 17 (2015) 68–77. http://dx.doi.org/10.1016/j.actbio.2015.01.024.

29. Obayi CS, Tolouei R, Mostavan A, Paternoster C, Turgeon S, Okorie BA, Obikwelu DO, Mantovani D. Effect of Grain Sizes on Mechanical Properties and Biodegradation Behavior of Pure Iron for Cardiovascular Stent Application. Biomatter (2016), 6:1, e959874.DOI:10.4161/21592527.2014.959874.

30. Robert De Angelis, Todd Snyder, Joel House, William Hosford. Quantitative description of fiber textures in cubic metals. Advances in X-ray Analysis, 1998, Vol.42, pp.510-520.

31. Lévesque J, Hermawan H, Dubé D, Mantovani D. Design of a pseudo-physiological test bench specific to the development of biodegradable metallic biomaterials. Acta Biomaterialia, 2008, 4(2), 284-295.

32. ASTM, Standard Test Method for Conducting Potentiodynamic Polarization Resistance Measurements. 2009.

33. George E. Dieter. Mechanical Metallurgy. McGraw-Hill Book Co., New York, 1986.

34. Hutchinson W.B. Recrystallization textures in Iron resulting from nucleation at grain boundaries. Acta Metall. 1989, 37(4), 1047-1056.

35. Dillamore I, Smith C, Watson T. Oriented nucleation in the formation of annealing textures in iron. Metal Science 1967;1:49-54.

36. Borbély A, Driver J, Ungár T. An X-ray method for the determination of stored energies in texture components of deformed metals; application to cold worked ultra high purity iron. Acta Materialia, 2000, 48, 2005-16.

37. Jai Gautam, Roumen Petrov, Leo KestensandElkeLunis, Surface energy controlled $\alpha-\gamma-\alpha$ transformation texture and microstructure character study in ULC steels alloyed with Mn and Al, Journal of Materials Science 43, 2008, 3969–3975.

38. T. Yamamoto, K. Fushimi, S. Miura, H. Konno. Effect of Cold Rolling on Passive Film on Pure Iron in pH 8.4 Borate Buffer Solution, ECS Transactions, 2010, 25 (40) 3-15 DOI: 10.1149/1.3422577.

39. Malgorzata R.G., Marzena P.R., Jerrzy K. Corrosion resistance and microstructure of steel AISI 316L after cold plastic deformation. Metallurgy & Foundry Engineering.2009, 35(1), 35 – 43.